



Suspension HVOF Spraying of Reduced Temperature Solid Oxide Fuel Cell Electrolytes

Jörg Oberste Berghaus, J.-G. Legoux, C. Moreau, R. Hui, C. Decès-Petit,
W. Qu, S. Yick, Z. Wang, R. Maric, and D. Ghosh

(Submitted April 29, 2008; in revised form August 19, 2008)

Metal-supported solid oxide fuel cells (SOFCs) composed of a $\text{Ce}_{0.8}\text{Sm}_{0.2}\text{O}_{2-\delta}$ (SDC) electrolyte layer and $\text{Ni-Ce}_{0.8}\text{Sm}_{0.2}\text{O}_{2-\delta}$ (Ni-SDC) cermet anode were fabricated by suspension thermal spraying on Hastelloy \times substrates. The cathode, a $\text{Sm}_{0.5}\text{Sr}_{0.5}\text{CoO}_3$ (SSCo)-SDC composite, was screen-printed and fired *in situ*. The anode was produced by suspension plasma spraying (SPS) using an axial injection plasma torch. The SDC electrolyte was produced by high-velocity oxy-fuel (HVOF) spraying of liquid suspension feedstock, using propylene fuel (DJ-2700). The emerging technology of HVOF suspension spraying was explored here to produce thin and low-porosity electrolytes in an effort to develop a cost-effective and scalable fabrication technique for high-performance, metal-supported SOFCs. In-flight particle temperature and velocity were measured for a number of different gun operating conditions and standoff distances and related to the resulting microstructures. At optimized conditions, this approach was found to limit material decomposition, enhance deposition efficiency, and reduce defect density in the resulting coating, as compared to previous results reported with SPS. Produced button cells showed highly promising performance with a maximum power density (MPD) of 0.5 W cm^{-2} at 600°C and above 0.9 W cm^{-2} at 700°C , with humidified hydrogen as fuel and air as oxidant. The potential of this deposition technique to scale-up the substrate size to $50 \times 50 \text{ mm}$ was demonstrated.

Keywords HVOF suspension spraying, reduced temperature solid oxide fuel cells, suspension thermal spraying

1. Introduction

Solid oxide fuel cells (SOFCs) are highly efficient power converting devices combining low pollution and high fuel flexibility. The key obstacles for the widespread implementation of SOFC technology are the high component and overall manufacturing costs, which are compounded by the technical requirements of high performance, long-term stability, thermal cycling capability, and short startup

This article is an invited paper selected from presentations at the 2008 International Thermal Spray Conference and has been expanded from the original presentation. It is simultaneously published in *Thermal Spray Crossing Borders, Proceedings of the 2008 International Thermal Spray Conference*, Maastricht, The Netherlands, June 2–4, 2008, Basil R. Marple, Margaret M. Hyland, Yuk-Chiu Lau, Chang-Jiu Li, Rogerio S. Lima, and Ghislain Montavon, Ed., ASM International, Materials Park, OH, 2008.

Jörg Oberste Berghaus, Bekaert Advanced Coatings NV, E3-Laan 75-79, Deinze 9800, Belgium; **J.-G. Legoux** and **C. Moreau**, Industrial Materials Institute, NRC, Boucherville, QC, Canada; and **R. Hui**, **C. Decès-Petit**, **W. Qu**, **S. Yick**, **Z. Wang**, **R. Maric**, and **D. Ghosh**, Institute for Fuel Cell Innovation, NRC, Vancouver, BC, Canada. Contact e-mail: jorg.oberste-berghaus@bekaert.com.

time (Ref 1). It is increasingly recognized that for small-stationary SOFC units and mobile systems (1–5 kW), such as SOFC-based auxiliary power units (APU) for cars and trucks, metal-supported SOFCs operating at temperatures far below the traditional 1000°C can offer many advantages over the conventional electrode or electrolyte-supported SOFCs (Ref 2). Reduced-temperature (RT) SOFC systems not only permit low-cost peripheral material (metal support and insulation), but also offer increased structural robustness, thermal stability, reduced degradation, and increased flexibility in design and assembly (Ref 3, 4).

Possible approaches to compensate for the increased resistance to ion transport at a lower operating temperature are to reduce the electrolyte thickness of the traditional yttria-stabilized zirconia (YSZ) layer to only a few microns and/or to use electrolyte materials of inherently higher ionic conductivity, such as, for example, scandia-stabilized zirconia (ScSZ) or samarium-doped ceria (SDC) (Ref 3).

Ultimately, to realize a high performance of metal-supported SOFCs, a thin, low-porosity, and fully crystalline electrolyte layer is essential to separate the fuel from the oxidant atmosphere (Ref 5, 6). Among the different fabrication technologies available, thermal spraying (TS) is gaining increasing attention due to its high deposition rates and scale-up capacity, as well as its potential to produce multiple SOFC components sequentially and directly on metallic substrates without the traditional and costly postsintering step (Ref 3, 7). However, significant challenges in TS for SOFC production remain, which are



primarily related to high coating thickness, residual porosity/defects, and thermal stresses.

As a promising extension of conventional thermal spraying, the use of a liquid feed carrier in suspension plasma spraying (SPS) permits feeding and spraying of much finer particles to form thinner coatings with more refined microstructure and grain size (Ref 8-10). In their previous work, the authors reported a metal-supported fuel cell with a samarium-doped ceria (SDC) electrolyte and NiO-SDC anode fabricated by suspension plasma spraying using an axial injection plasma torch (Axial III, Northwest Mettech, North Vancouver, Canada). The cell showed promising performance at 650 °C with a MPD of 0.216 W cm⁻² and an open cell voltage (OCV) of 0.768 V (0.94 V theoretical OCV). Its resistance to oxidation and to rapid thermal cycling was evaluated (Ref 11).

The small particles created in SPS carry little momentum and low thermal inertia. They generally have to be heated far above their melting point in the high-temperature plasma ($T_{\text{flame}} > 8000$ °C) to retain the melting temperature and high velocity further downstream at the impact on the substrate to form a dense coating. For ceria, this high superheating in the chemically reducing plasma can lead to an undesirable transformation of CeO₂ to Ce₂O₃, which is associated with a lowering of the melting and boiling points (Ref 12). The decomposition and resulting vaporization can limit deposition efficiency, electrochemical performance, and mechanical integrity of the electrolyte. Employing a much lower flame temperature of a high-velocity oxy-fuel (HVOF) system (2600-3200 °C) may alleviate these effects, under the condition that the ceria particles are still heated to at least their melting point (~2730 °C) (Ref 12). Maximum particle temperatures in HVOF depend on a number of factors, including the torch design, the fuel and fuel-to-oxygen ratio, the feedstock and feed rate, and the position in the flame. Using acetylene, a high-energy fuel with some safety restrictions, HVOF suspension spraying of alumina, titania, and zirconia ceramics was recently reported at the University of Stuttgart (Ref 13). Advantages of HVOF spraying of conventional feedstock powders for SOFC production were also demonstrated (Ref 5). The authors reported earlier on suspension HVOF spraying of ceramic composites using more standard fuels (Ref 10). In this paper, HVOF suspension spraying for the production of ceria-based electrolyte coatings and the role of operating parameters on the in-flight particle states and microstructure are discussed. A metal-supported fuel cell was produced and its electrochemical performance was evaluated.

2. Experimental Procedure

2.1 Spray Systems and Materials

Suspension spraying for the SDC coatings was implemented using an HVOF DJ-2700 hybrid gun (Sulzer-Metco, Westbury, NY) using propylene fuel (C₃H₆). The system was equipped with an internal injection/atomization module inserted into the standard powder feeding port, thereby intimately contacting the coaxially

Table 1 DJ-2700 HVOF spray parameters

Parameter	Value
Propylene flow	90, 85, 75, and 70 slpm
Oxygen flow	279 slpm
Air flow	202 slpm
Carrier gas (N ₂) flow	15 slpm
Spray distance	7.6-12.7 cm
Gun traverse speed	762 mm/s
Suspension solid content	2.5-5 wt.%
Suspension feed rate	25-50 mL/min

fed suspension droplets with the fuel inside the HVOF combustion chamber. The suspension was delivered by a prototype Nanofeed Liquid Powder Feeder (Model 640, Northwest Mettech). Flow-rate control, start-up, shut-down, and rinsing sequences are fully automated and PC controlled. The injection module and fuel distributor were continuously cooled with nitrogen. The system delivered the suspension feed against the combustion backpressure of up to 6.46 atm. HVOF operating conditions, used in this experiment, are summarized in Table 1.

In-flight particle states were measured with a commercial diagnostic system (AccuraSpray[®] G2 Tecnar, St-Bruno, PQ, Canada). The temperature measurement is based on two-color pyrometry, and the velocity is determined by a time-of-flight technique. Microstructures of the coatings were observed by FEG-SEM (Hitachi S4700). The samples were prepared by standard metallographic methods. Porosity was assessed on the cross-section microstructure images taken by SEM (5000×), and then using image analysis.

Phase analysis was carried out by XRD using a Bruker D8-Discovery diffractometer (Bruker AXS Inc. Madison, USA) with Cu K α radiation at 0.01°/s. The crystallite size was approximated from the Sherrer equation at the principal diffraction lines.

For the electrolyte coatings, two different Ce_{0.8}Sm_{0.2}O_{2- δ} feedstock powders were used, namely, a micron-sized powder (d_{50} , 1.45 μ m) with a specific surface area (SSA) of 5.37 m²/g (Nextech Materials, Lewis Center, OH) and nanosized powders with SSA of 80-220 m²/g (nGimat, Atlanta, GA), having a particle size of approximately 20 nm, which was estimated from the crystallite size as measured by XRD. Suspensions of initially 5 wt.% and then 2.5 wt.% solids were prepared in a mixture of ethanol and ethylene glycol. The nanosized powder was prone to form aggregates in the suspension. Wide-size distributions with aggregate ranging from 40 nm (lower detection limit) to 10 μ m were measured with a Coulter LS Particle size analyzer (Beckman Coulter Canada Inc., Mississauga, CAN) using a liquid module in highly diluted aqueous suspensions. Polyethylenimine (MWT 25,000 Alfa Aesar, USA) was used as dispersing agent. It was found that the addition of viscous ethylene glycol further prolonged the settling time of the suspension. Most coatings were produced on steel substrates or functional anodes disks of 16 mm diameter (button cells). Electrolyte coatings were also produced on larger substrates with rectangular dimension of 50 × 50 mm. Surface temperatures, as

monitored by a pyrometer, were controlled during deposition, using a specialized substrate holder.

2.2 Substrate and Anode

Tape cast and sintered Hastelloy \times plates (Mott Corp., Farmington, CT) were used as metallic substrates. A substrate porosity of 16% was determined by image analysis.

NiO-SDC (50 wt.% NiO) anodes were produced by suspension plasma spraying using a torch with three converging plasma jets and an axial feed injection port (Axial III, Northwest Mettech). Relatively large NiO powders (d_{50} , 14.4 μm ; SSA, 0.21 m^2/g) and micron-sized SDC powders (d_{50} , 1.2 μm ; SSA, 8.9 m^2/g) (Nextech Materials, Lewis Center, OH) were used as feedstock. In an attempt to produce a relatively porous anode layer, while fully covering the substrate pores, spray conditions were selected to provide high particle velocities (700 m/s), but relatively low particle temperatures (2400 °C). These particle states were attained at a high plasma gas flow rate (275 slpm) and by using helium as the secondary gas at 30%, with argon and nitrogen as balance. Furthermore, the suspensions in 30 wt.% ethylene glycol in ethanol were fed at a high rate (70 mL/min), thereby imposing a high thermal load on the plasma flame. The anodes were produced at a spray distance of 62.5 mm with maximum surface temperature of 300 °C. Further details can be found elsewhere (Ref 14). After deposition, the NiO was reduced to Ni at 600 °C in hydrogen for 30 min, thereby inducing the first and possibly most significant volume change in the fine-grained anode. This additional process step was previously found to reduce crack formation in the electrolyte during SOFC testing (Ref 11). Large surface humps on the anode, which can sometimes occur in suspension spraying, were removed by mechanic polishing.

2.3 Cathode Deposition and Cell Testing

After electrolyte deposition, a $\text{Sm}_{0.5}\text{Sr}_{0.5}\text{CoO}_3$ (SSCo)-SDC (weight ratio 70:30) composite cathode was stencil printed on the half cell and fired *in situ* at 800 °C for 2h. To further reduce the anode, the cell was then maintained at 650 °C for 5h while gradually introducing hydrogen. The power generation characteristics were measured from 500 to 700 °C in 50 °C intervals. At each temperature, electrochemical performance and ac impedance measurements were performed twice using humidified hydrogen (3% H_2O) as fuel and air as oxidant. Before cathode deposition, the half cells were subjected to a helium leak test at 0.0689 bar differential pressure. Details on the testing setup for gas permeability and electrochemical performance are published elsewhere (Ref 11).

3. Results and Discussion

3.1 Initial Tests

Initial tests of HVOF suspension spraying with SDC revealed limited, if any, coating deposition. A typical example of a microstructure of these early coatings, using

the larger micron-sized SDC feedstock, is shown in Fig. 1(a). A 5 wt.% SDC suspension in ethanol was fed at a feed rate of 50 mL/min. The propylene flow was 80 slpm and the spray distance 12 cm. The microstructure in the backscattered electron image features regions of gray contrast, which can be interpreted as pull-out and fracture surfaces created during the polishing step, indicative of limited material fusion. Individual particles can be discerned, which resemble unmolten feed particles. The flame enthalpy was likely insufficient to melt most of the micron-sized ceria particles. Similar observations are reported for high velocity suspension flame spraying of zirconia (Ref 13). Another example, using the much finer nanosized SDC feedstock dispersed as 5 wt.% in ethanol and fed at 50 mL/min, is shown in Fig. 1(b) and (c). This coating was deposited with 80 slpm propylene flow at a standoff distance of 10 cm on a stainless steel 430 substrate. Some isolated regions of dense material can be discerned. A higher degree of particle melting possibly occurred with the fine particles due to the higher surface area available for heat transfer and lower melting times of the smaller material volume. However, the coating is strongly fractured and the material appears to adhere only by virtue of mechanical anchoring between the roughness asperities of the substrate. Again, regions of gray contrast are indicative of limited material melting and fusion and limited splat contact due to a low flame enthalpy.

3.2 Spray Distance

In-flight particle states as a function of standoff distance are exemplified in Fig. 2 at the spray condition for the coating from the nanosized SDC in Fig. 1(b) and (c), i.e., 80 slpm C_3H_6 . At the spray distance (SD) used in the initial test, i.e., 10 cm, the average particle temperature of 2550 °C was far below the melting point of ceria and the velocity was as high as 800 m/s. These values support the idea that most particles were indeed unmelted and that their impact at high velocity contributed to the cracking and material removal by grit blasting, consistent with the observed microstructure.

It is interesting to note that the maximum average particle temperature was measured far downstream from the gun nozzle exit (16 cm). At SD of 10 cm, the particles are still in a process of heating in the supersonic flame. This suggests that, in this example, they have not experienced temperatures higher than approximately 2650 °C during their in-flight history, including inside the HVOF combustion chamber. In principle, vaporization and decomposition due to superheating of the ceria particles, as it can occur in plasma spraying, are avoided by the inherently imposed upper temperature limit of the HVOF system. The diagnostic system indirectly provided evidence for less vaporization by capturing a meaningful signal, which was previously distorted in plasma spraying due to the spectral emission of evaporating ceria (Ref 14).

Using the on-line diagnostics, subsequent efforts were focused on increasing the particle temperature by adjusting the operating and feed conditions using the nanosized SDC feedstock.

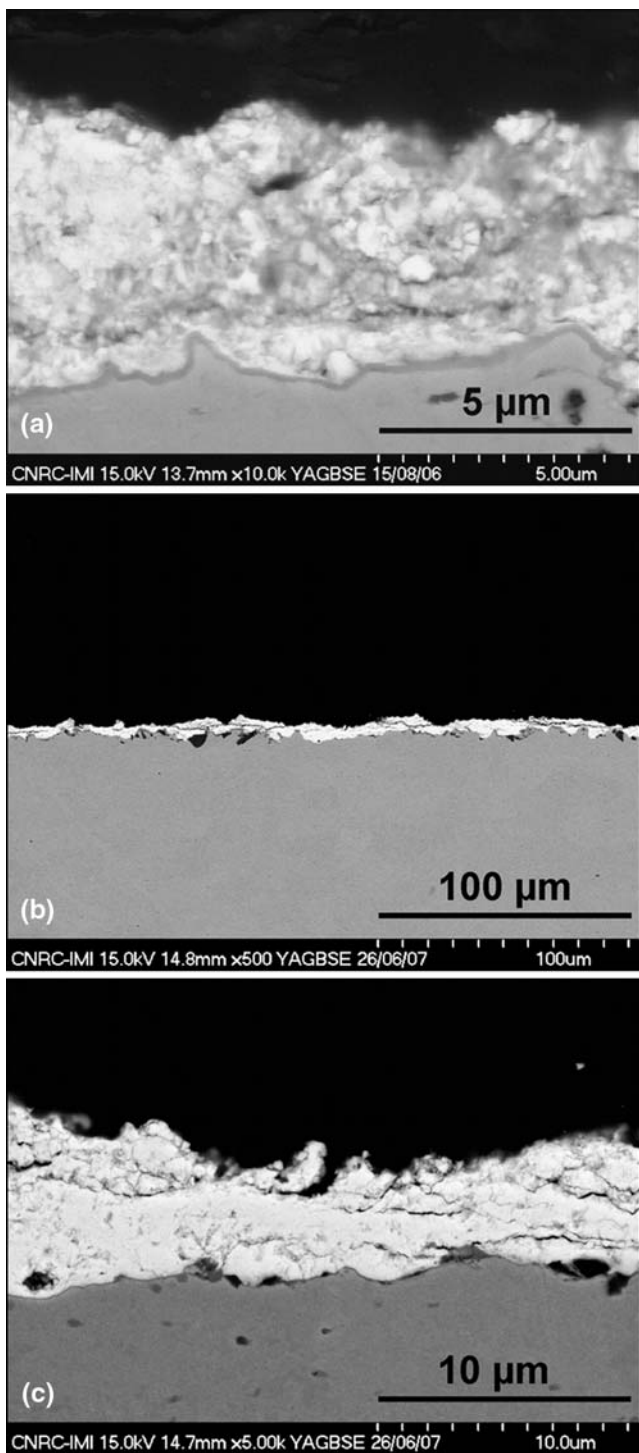


Fig. 1 Microstructure of initial HVOF SDC coating from (a) micron-sized and (b, c) nanosized feedstock

3.3 Fuel-to-Oxygen Ratio

Figure 3 exemplifies the effect of propylene fuel rates at constant measurement distance (127 mm), oxygen flow, and two slightly different suspension feed conditions (A&B), i.e., 5 wt.% solid suspension in ethanol at

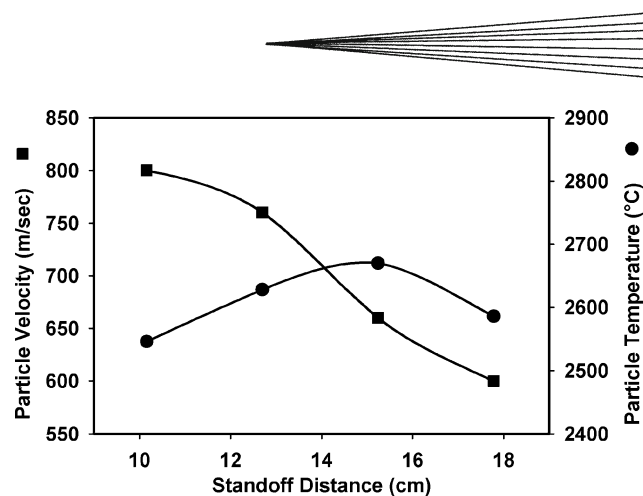


Fig. 2 Axial T-V profile at suboptimal conditions

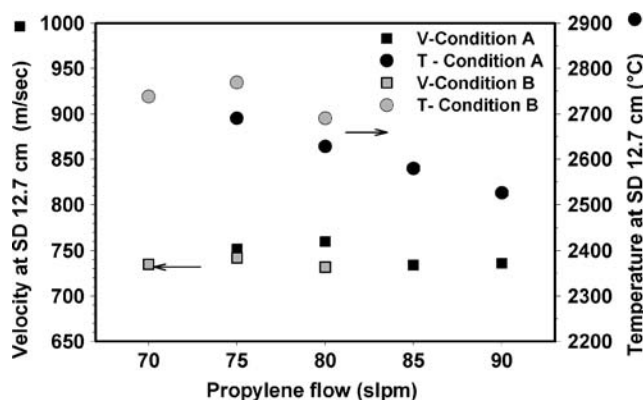


Fig. 3 Effect of propylene flow on particle T and V

50 mL/min without (A) and with the addition of 50% ethylene glycol (B). While the particle velocity remained essentially constant, higher particle temperatures were attained at lower fuel rates, approaching those of the stoichiometric oxygen/fuel ratio of 4.5 to 1. Considering that both entrained shroud air and the suspension solvent can contribute to the combustion, the most efficient conditions may shift from stoichiometry. A maximum particle temperature was generally obtained with over-stoichiometric fuel supply, as in the example of condition B in Fig. 3.

3.4 Suspension Feed Rate

Figure 4 exemplifies the effect of the suspension feed rate at constant spray conditions (85 slpm C_3H_6 , SD 127 mm) and suspension composition (5 wt.% solids in ethanol). The observed increase in particle temperature and velocity with decreasing feed loading is typical for suspension thermal spraying (Ref 9). In SPS, this is mainly associated with the lowering of the heat requirement for evaporation of the suspension medium. Such loading effect was expected to be less pronounced in HVOF suspension spraying, since the combustion of the ethanol solvent in intimate contact with the particles could partially compensate for heat loss by evaporation. In this

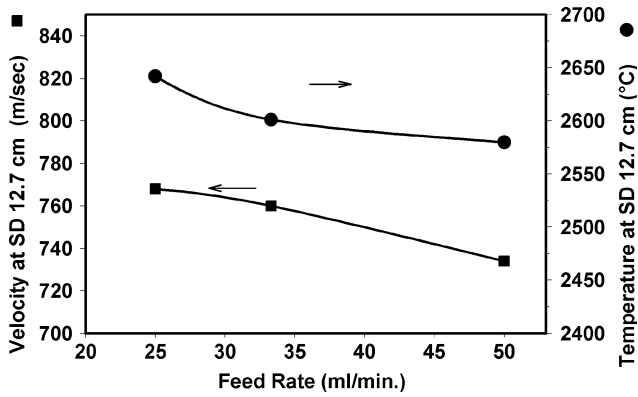


Fig. 4 Effect of feed rate on particle T and V

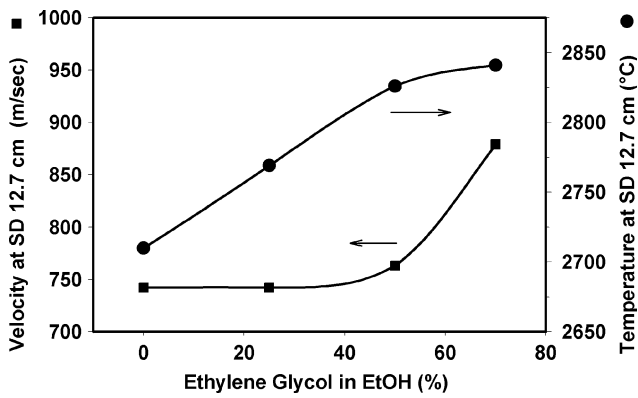


Fig. 5 Effect of ethylene glycol to ethanol ratio

case, however, the flame was already fuel rich and the ethanol may not have significantly contributed to the combustion heat.

3.5 Nature of Suspension Solvent

Figure 5 shows the effect of adding ethylene glycol (EG) to the ethanol-based suspension solvent at different mixing ratios, keeping the torch operating conditions (75 slpm C_3H_6 , SD 127 mm) and feed conditions (5 wt.% solids at 50 mL/min) constant. The high boiling point glycol (B.P. 197.3 °C) has both a slightly higher vaporization enthalpy (63.9 kJ/mol) and a lower heat of combustion (19.8 kJ/g) than ethanol ($\Delta_{vap}H_{(25^\circ C)}$ 42.32 kJ/mol, $\Delta_c H^\circ$ 29.87 kJ/g). Increasing particle temperature and velocity with increased EG content was consequently somewhat surprising. A possible explanation may be an improved dispersion of the particles in the viscous glycol suspension ($\eta \sim 16.1$ mPa s) as compared to ethanol ($\eta \sim 1.2$ mPa s), which may stabilize the suspension to form smaller aggregates, which may then translate, in average, into smaller in-flight particles created during the atomization and solvent combustion step. In SPS the agglomerate distribution in the feed plays an important role in their transformation into ceramic droplets (Ref 8, 10). Smaller particulates, in turn, are more readily heated and

Table 2 Optimized spray parameters for SDC electrolyte

Parameter	Value
Propylene flow	75 slpm
Oxygen flow	279 slpm
Air flow	202 slpm
Carrier gas (N_2) flow	15 slpm
Spray distance	12.7 cm
Gun traverse speed	762 mm/s
Suspension solid content	2.5 wt. %
Suspension feed rate	33 mL/min
Particle size	~ 20 nm SDC
Suspension composition	70/30 wt. % glycol/ethanol

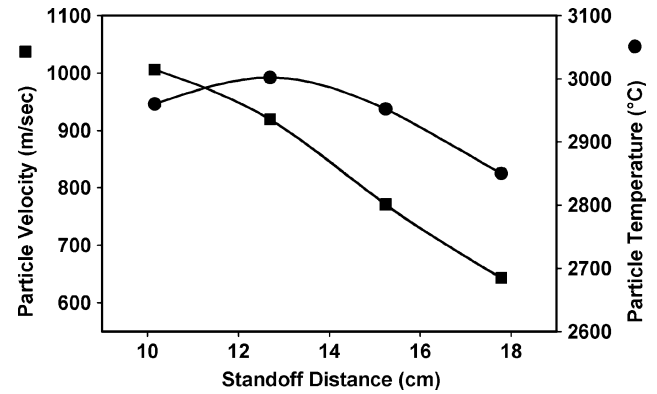


Fig. 6 Axial T-V profile at optimum spray conditions for SOFC production

melted and accelerated to the gas velocity, as explained earlier. Following this reasoning, lowering the solid content in the suspension from 5 to 2.5 wt.% may also improve the particle dispersion or, at least, slow down the formation of larger aggregates during processing by providing a longer mean-free path for particle/aggregate collisions. A lower solid content is further expected to decrease the heat load on the flame available for particle melting and heating. Based on the findings, optimized spray conditions were established for the nanosized SDC feedstock at slightly over-stoichiometric propylene flow, low suspension feed rate and solid loading and with high glycol content, as summarized in Table 2. At these conditions an average particle temperature close to 3000 °C was measured. The corresponding T-V profile as a function of SD is shown in Fig. 6.

3.6 As-Sprayed SOFC Half Cell

By positioning the substrate at the highest measured particle temperature (127 mm) at the optimized conditions, SDC electrolytes (~ 20 μ m thick) were deposited on 50-60 μ m thick anode layers supported by 16 mm diameter Hastelloy \times substrates. A surface temperature of 450 °C was maintained. Figures 7 and 8 show cross-sectional micrographs of the as-sprayed cell, without the cathode. The electrolyte has a relatively dense microstructure (no visible open porosity and closed porosity

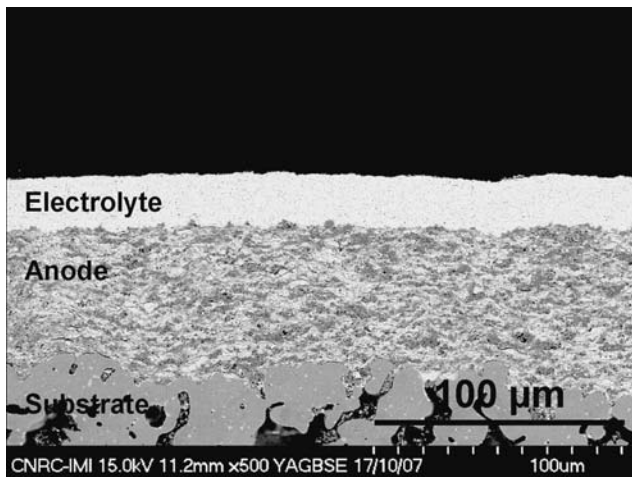


Fig. 7 Microstructure of HVOF sprayed half cell

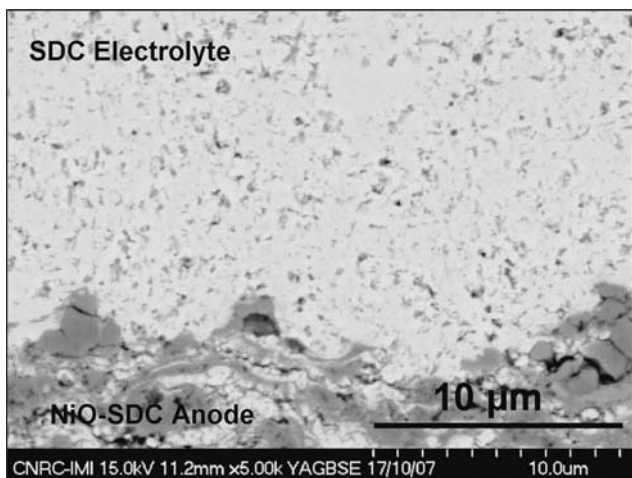


Fig. 8 As-sprayed SDC-NiO/SDC microstructure

<2% as estimated from cross-section SEM image analysis). A lamellar structure, typical for thermal sprayed coatings, cannot be discerned. The SDC layer also appeared well adherent to the anode. The backscattered electron image shows only few gray contrasted fracture and pull-out regions, which is indicative of a high degree of material fusion. The lack of gray regions may also suggest the absence of Ce_2O_3 phases. XRD analysis indicated that the crystal structure was exclusively doped cerianite (CeO_2) with a grain size of approximately 37 nm. It was noted that the electrolyte was virtually free of cracks or pinholes. Gas permeability below 0.1 slpm/cm^2 was determined under helium pressure (6.89 kPa). In thermal spraying, tensile stresses generally arise due to the material shrinkage during solidification and cooling of the molten droplets, often leading to transverse cracks. Using HVOF, these stresses may be partially compensated by the plastic deformation of unmolten or partially molten ceramic particles impacting at high velocity (Ref 5). At the

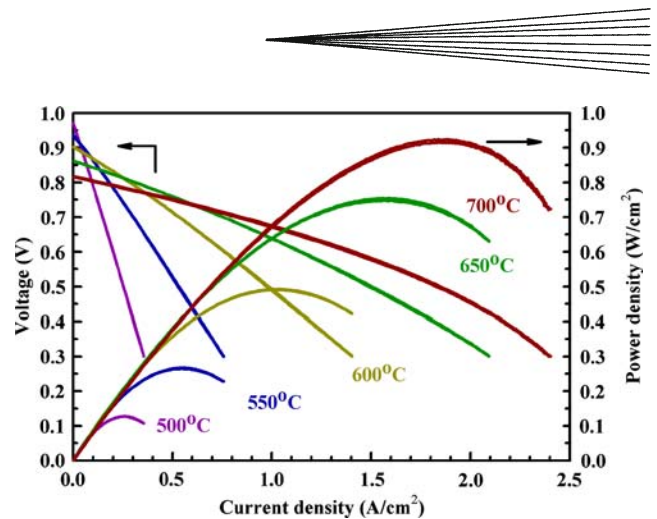


Fig. 9 Performance of HVOF sprayed SOFC

spray conditions used, a substantial portion of the particles were likely not fully molten and their impact at nearly 900 m/s may have affected the intrinsic stresses by introducing a compressive component. Furthermore, the top surface of the electrolyte was relatively smooth without the humps and defects often seen in SPS (Ref 10). The impacting colder particles may remove loosely attached material during deposition leading to this low surface roughness.

3.7 SOFC Cell Performance

After cathode deposition, the cell performance and impedance was tested from 500 to 700 °C, as described above. Figure 9 shows an open circuit voltage (OCV) of 0.97 V at 500 °C, nearly 90% of the theoretical OCV value of 1.08 V (Ref 15). The OCV then decreases with temperature due to the rise in electronic contribution to the SDC conductivity (Ref 4). The maximum power density increases continuously to 0.49 W cm^{-2} at 600 °C and up to 0.92 W cm^{-2} at 700 °C. This performance compares very favorably with the previous results of the authors (Ref 11), as well as other published results for metal-supported SOFCs (Ref 3, 7) in the reduced temperature range, of which the authors are aware. Figure 10 summarizes the area specific resistances (ASRs). Above 600 °C, the contribution of the polarization resistance to the total resistance is almost negligible. This suggests that catalytic activity of the electrodes is not a limiting factor. At lower temperatures, however, both ohmic and polarization resistance rise significantly. Ohmic resistance is generally attributed to restricted ion conductivity through the electrolyte and may be a consequence of the residual pores/imperfect splat contact in the coating, at least in comparison with fully sintered bulk-like ceramic (Ref 4). On the other hand, an imperfect contact between the electrolyte and the electrodes may also contribute to both polarization and ohmic resistance. Indeed, the interfaces proved to be of limited quality. Thermal cycling tests at a heating rate of 60 °C/min , i.e., heating the cell from 25 to 600 °C in 10 min multiple times, revealed a significant degradation at the cathode-electrolyte interface with a

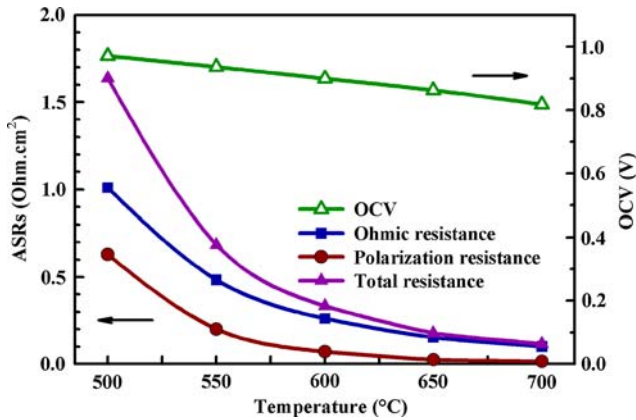


Fig. 10 Area specific resistances (ASR) and OCV

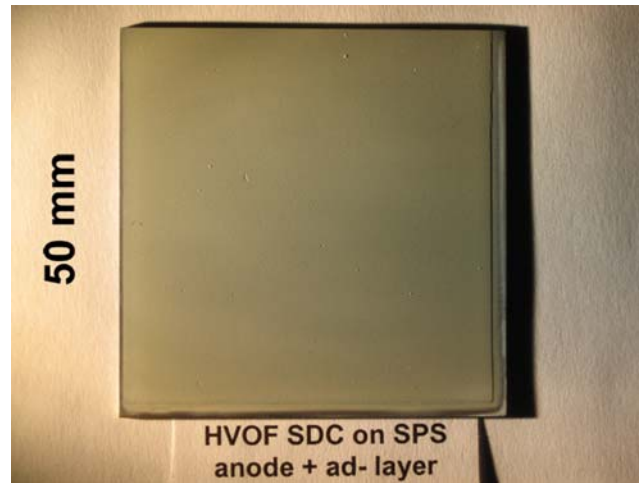


Fig. 12 Top-view of 50 × 50 mm half cell

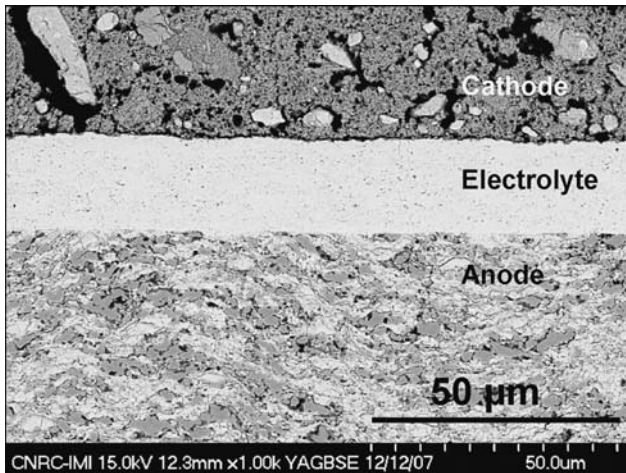


Fig. 11 SOFC after testing and thermal cycling

strong increase in overall cell resistance. The OCV remained stable throughout the tests. Further details will be presented elsewhere. Figure 11 shows the cell cross section after testing and thermal cycling. While the electrolyte appears unaltered, which is consistent with the constant OCV, a partial separation of the electrolyte from the cathode can be discerned. This degradation was previously observed in the SPS cells and was attributed to the mismatch in thermal expansion coefficient between the layers (Ref 11). Development of more suitable electrodes is in progress.

3.8 Short Stack Components (5 × 5 cm)

To assess the potential for planar SOFC stack production, half cells with rectangular dimensions of 50 × 50 mm were produced. Without optimizing for the deposition rate, the electrolyte coating was deposited in 16 min, consuming approximately 13.3 g of feedstock powder. This relatively high deposition rate, in comparison with the previous SPS tests conducted by the authors,

may be allocated to the low flame temperature, which precludes feedstock evaporation. Figure 12 shows a top-view photograph of an as-sprayed functional electrolyte-anode-metal assembly. In spite of the relatively high surface temperature (440 °C) and the localized heating by the impinging spray jet, the samples did not show any distortion during or after spraying. Furthermore, no optical visible defects in the electrolyte coating were detected. Electrochemical characterization of the cell is in progress at the time of writing. Deposition at relatively large standoff distances (~13 cm) was made possible by the ongoing heating of the particles far outside the HVOF gun as they approach the substrate, see Fig. 2 and 6. This stands in contrast to SPS, where the small particles cool rapidly after exiting the torch and the substrate must consequently be placed in close proximity to the plasma (Ref 11). In HVOF suspension spraying, the thermal stresses and local overheating, a severe limitation for atmospheric pressure thermal spraying of SOFC electrolytes (Ref 3), promise to be manageable.

4. Conclusions

Suspension HVOF spraying (DJ-2700) for the production of ceria-based SOFC electrolytes was implemented. Using in-flight particle diagnostics, optimum spray parameters in terms of fuel-to-oxygen ratio, feedstock/suspension conditions, and standoff distance were established. The HVOF flame was found to limit evaporation and decomposition of the feedstock and to favorably affect the coating stresses, resulting in low-porosity, smooth, and virtually defect-free coatings of ~20 μm thickness. The flame characteristics allow for relatively large standoff distance to facilitate thermal management of the substrate. The cells showed high performance with a MPD of 0.49 W cm⁻² at 600 °C and above 0.9 W cm⁻² at 700 °C. Ongoing work focuses on improving component compatibility and long term stability.



Acknowledgments

The financial support by the National Fuel Cell and Hydrogen Program of the National Research Council of Canada is greatly acknowledged.

References

1. E. Ivers-Tiffée, A. Weber, and D. Herbstritt, Materials and Technologies of SOFC-Components, *J. Eur. Ceram. Soc.*, 2001, **21**, p 1805-1811
2. N.P. Brandon, D. Corcoran, D. Cummings, A. Duckett, K. El-Khoury, D. Haigh, R. Leah, G. Lewis, N. Maynard, T. McColm, R. Trezona, A. Selcuk, and M. Schmidt, Development of Metal Supported Solid Oxide Fuel Cells for Operation at 500-600 °C, *J. Mater. Eng. Perform.*, 2004, **13**(3), p 253-256
3. R. Henne, Solid Oxide Fuel Cells: A Challenge for Plasma Deposition Processes, *J. Therm. Spray Technol.*, 2007, **16**(3), p 381-402
4. X. Zhang, M. Robertson, C. Decès-Petit, Y. Xie, R. Hui, S. Yick, E. Styles, J. Roller, O. Kessler, R. Maric, and D. Ghosh, NiO-YSZ Cermet Supported Low Temperature Solid Oxide Fuel Cells, *J. Power Sources*, 2006, **161**, p 301-307
5. R. Gadow, A. Killinger, A. Candel Ruiz, H. Weckmann, A. Öllinger, and O. Patz, Investigation on HVOF Technique for Fabrication of SOFCs (Solid Oxide Fuel Cells) Electrolyte Layers, *Proceedings of the 2007 International Thermal Spray Conference, Global Coatings Solutions*, May 14-16 2007 (Beijing, China), ASM International, 2007, p 1053-1058
6. D. Stöver, Dag Hathiramani, R. Vaßen, and R.J. Damani, Plasma-Sprayed Components for SOFC Applications, *Surf. Coat. Technol.*, 2006, **201**, p 2002-2005
7. R. Hui, Z. Wang, O. Kessler, L. Rose, J. Jankovic, S. Yick, R. Maric, and D. Ghosh, Thermal Plasma Spraying for SOFCs: Applications, Potential Advantages, and Challenges, *J. Power Sources*, 2007, **170**, p 308-323
8. P. Fauchais, R. Etchart-Salas, C. Delbos, M. Tognonvi, V. Rat, J.F. Couder, and T. Chartier, Suspension and Solution Plasma Spraying of Finely Structured Layers: Potential Application to SOFCs, *J. Phys. D.: Appl. Phys.*, 2007, **40**, p 2394-2406
9. J. Oberste Berghaus, S. Bouaricha, J.-G. Legoux, C. Moreau, and T. Chráska, Suspension Plasma Spraying of Nano-Ceramics Using an Axial Injection Torch, *Proceedings of the 2005 International Thermal Spray Conference, Thermal Spray: Building on 100 Years of Success*, May 2-5, 2005 (Basel Switzerland), ASM International, 2005, p 1434-1440
10. J. Oberste Berghaus, J.G. Legoux, C. Moreau, F. Tarasi, T. Chraska, Mechanical and Thermal Transport Properties of Suspension Thermal-Sprayed Alumina-Zirconia Composite Coatings, *J. Therm. Spray Technol.*, 2008, **17**(1)
11. Z. Wang, J. Oberste Berghaus, S. Yick, C. Decès-Petit, W. Qu, R. Hui, R. Maric, and D. Ghosh, Dynamic Evaluation of Low-Temperature Metal-Supported Solid Oxide Fuel Cell Oriented to Auxiliary Power Units, *J. Power Sources*, 2008, **176**(1), p 90-95
12. S. Sodeoka, M. Suzuki, K. Ueno, H. Sakuramoto, R. Shibata, and M. Ando, Thermal and Mechanical Properties of ZrO₂-CeO₂ Plasma-Sprayed Coatings, *J. Therm. Spray Technol.*, 1997, **6**(3), p 361-367
13. A. Killinger, M. Kuhn, and R. Gadow, High-Velocity Suspension Flame Spraying (HVSFS), A New Approach for Spraying Nanoparticles with Hypersonic Speed, *Surf. Coat. Technol.*, 2006, **201**, p 1922-1929
14. J. Oberste Berghaus, J.-G. Legoux, C. Moreau, R. Hui, and D. Ghosh, Suspension Plasma Spraying of Intermediate Temperature SOFC Components Using an Axial Injection DC Torch, *Mater. Sci. Forum, Trans. Tech. Publisher, Switzerland*, 2007, **539-543**, p 1332-1337
15. T. Matsui, T. Kosaka, M. Inabe, A. Mineshige, and Z. Ogumi, Effects of Mixed Conduction on the Open-Circuit Voltage of Intermediate-Temperature SOFCs Based on Sm-Doped Ceria Electrolytes, *Solid State Ionics*, 2005, **176**, p 663-668